ACS APPLIED MATERIALS & INTERFACES

Research Article

www.acsami.org

High-Performance of PEDOT/PSS Free Organic Solar Cells on an Air-Plasma-Treated ITO Substrate

Jong Kil Choi, Ming Liang Jin, Cheng Jin An, Dae Woo Kim, and Hee-Tae Jung*

Department of Chemical and Biomolecular Engineering, Korea Advanced Institute of Science and Technology, 335 Gwahangno, Yuseong-gu, Daejeon 305-701, Korea

Supporting Information

ABSTRACT: In this work, we demonstrate the high-performance of a PEDOT:PSS free organic photovoltaic cell (OPVC) using an air-plasma modified ITO surface, followed by controlled solvent evaporation and annealing of the P3HT:PCBM photoactive layer. Ultraviolet photoelectron spectroscopy (UPS), X-ray photoelectron spectroscopy (XPS), and conductive atomic force microscopy (c-AFM) results show that the work function of ITO was increased to as high as that of PEDOT:PSS (5.2 eV) after air-plasma treatment, along with significantly enhanced electrical homogeneity. From the dynamic secondary ion mass spectroscopy (DSIMS) results, we confirm that the thermodynamic stability of the slow-dried active layer is attributed to the uniform vertical compositional distribution on the air plasma treated ITO surface, even after thermal annealing at 150 °C for 10 min. The resulting device has an open-circuit voltage of 0.65 V, a fill factor of 63%, and a power conversion efficiency of 3.38%, providing a high performance PEDOT:PSS free OPVC device.

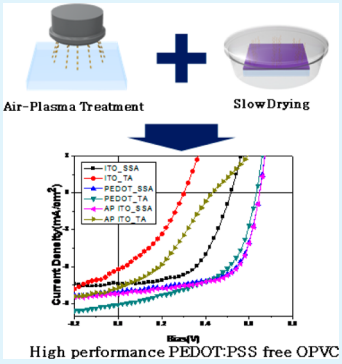

KEYWORDS: *surface modification of ITO, PEDOT:PSS free, phase separation, organic photovoltaic cell*

INTRODUCTION

Bulk heterojunction (BHJ) systems are composed of a bicontinuous composite of donor and acceptor phases and are one of the most well-known organic photovoltaic cells (OPVC). This is because the large interfacial areas between the donors and acceptors allow for efficient exciton dissociation.[1−7] In the simplest bulk heterojunction system, a blended solution of electron donor and acceptor materials is typically spin-cast onto a transparent anode. Both components interpenetrate one another, thereby maximizing the interfacial area where dissociation of excitons takes place. However, because of the disordered nature of the BHJ system, a hole transporting layer (HTL) (or electron blocking layers, EBL) is required between the transparent conductive indium tin oxide (ITO) anode and the photoactive layer for effective hole collection.[8−11] This requirement is a consequence of direct contact of the donor and acceptor materials with the anode, leading to current leakage, and the recombination of carriers.

Semiconducting poly(3,4-ethylenedioxythiophene):poly-(styrenesulfonate) (PEDOT:PSS) has been primarily used as a HTL layer because of its solution processability, effective electron blocking, and hole transportation properties.[8] Despite such advantages, it is known that PEDOT:PSS corrodes ITO due to its highly acidic (~pH 1) aqueous suspension, and can also introduce water into the photoactive layer, leading to the degradation of the device performance.[12−14] Furthermore, the PEDOT:PSS layer may induce inhomogeneous electrical properties and inconsistent film morphologies.[15,16] These limitations have driven the development of better interfacial tailoring methods which can give rise to the necessary electronic properties, allowing PEDOT:PSS to be replaced.

Two different approaches have been suggested to replace PEDOT:PSS. These include the incorporation of transition metal oxides with high work functions (MoO_3, V_2O_5, WO_3, and NiO) and surface treatments of ITO.[9,10,17−20] The n-type electronic character and exceptionally deep lying electronic states of transition metal oxides makes them very effective hole injection and extraction layers. However, the use of transition metal oxides as a HTL layer can allow for the evaporative formation of films under high vacuum conditions, which is a critical limitation.

The surface treatment of ITO is particularly interesting because it is very simple and cost-effective, and does not require any additional materials such as PEDOT:PSS and transitional metal oxides.[21,22] It is required that the surface modified ITO create ohmic contact for effective hole extraction, and minimize the detrimental effects that arise from an inhomogeneous ITO surface. The ohmic contact between the anode and the HOMO of the donor material provides efficient charge collection without energy loss or a Schottky barrier.[21] However, the electrical inhomogeneity of the ITO surface that arises from the uneven distribution of the atomic composition and carbon contamination can create a multitude of surface states, consequently reducing V_{oc} and increasing the series resistance.[21,23]

The surface of ITO has been primarily modified by (i) acid treatment using an aqueous HCl solution followed by ultraviolet ozone (UVO) irradiation and (ii) surface mod-

Received: November 13, 2013
Accepted: July 2, 2014
Published: July 2, 2014

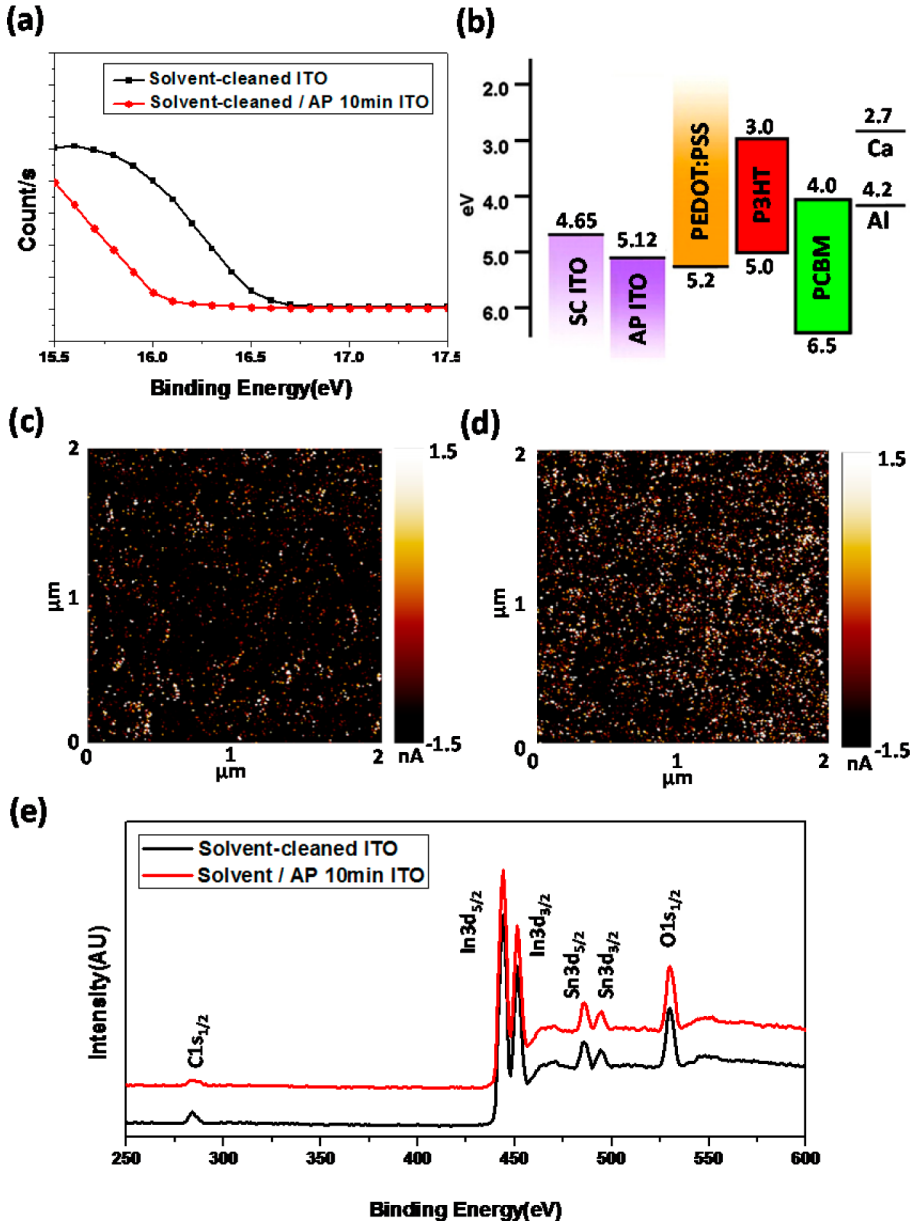

Figure 1. (a) UPS spectra of the solvent-cleaned (SC) ITO surface (black), and the solvent-cleaned ITO surface that was treated with air plasma (AP) for 10 min (red). Solvent-cleaned ITO was cleaned with a combination of acetone, DI water, and IPA. (b) Schematic energy level diagram. c-AFM images of (c) SC ITO and (d) SC/AP treated ITO. (e) X-ray photoelectron spectroscopy (XPS) spectra of the ITO surface treated with SC (black) and SC/AP (red).

ification using self-assembled monolayers (SAMs).[21,22] It has been shown that the electrical homogeneity of the ITO surface was enhanced greatly after combined HCl and UVO treatments, resulting in a reduced charge trap density and an improved V_{oc} and FF.[21] Similarly, surface modification using a SAM material which has an electron-withdrawing and hydrophobic CF_3 terminal group on the ITO surface increases the ITO work function, allowing for better ohmic contact between the electrode and the donor material, and effectively reducing extreme phase separation at the anode interface.[22]

Previous studies have also addressed the use of air plasma treatment of ITO to increase the work function to values as high as that of PEDOT:PSS (5.2 eV), which is accompanied by significant surface electrical homogenization.[24,25] These results suggest that an air plasma treated ITO surface is capable of creating an ohmic contact to a P3HT donor material with an increased electroactive surface area. However, the interfacial instability and decohesive force between the hydrophilic air plasma treated ITO and a hydrophobic photoactive layer induces excessive phase separation at the anode interface, especially at elevated temperatures, consequently reducing the performance of the OPVC.[26,27] Therefore, reducing the interfacial instability induced by the large surface energy difference is essential for replacing the PEDOT:PSS layer with air-plasma treated ITO.

In this work, we modified an ITO surface using air-plasma treatment to fabricate a high performance PEDOT:PSS free OPVC, followed by controlled solvent annealing of the P3HT:PCBM blend on the air-plasma treated ITO. It was found that the work function of ITO increased to as high as that of PEDOT:PSS (5.2 eV) after the air-plasma treatment, and significantly enhanced electrical homogeneity was achieved.

More importantly, we found that the slow solvent drying of the P3HT:PCBM layer on the air-plasma treated ITO surface significantly reduced the interfacial instability between the air-plasma treated ITO and the photoactive layer, leading to optimized phase separation near the plasma-treated ITO surface. The resulting PEDOT:PSS free OPVC exhibits high performance device characteristics, which offers great potential for the fabrication of simple and inexpensive solar cells.

EXPERIMENTAL SECTION

Device Fabrication. The ITO-coated glass was cleaned sequentially with acetone, deionized water, and isopropyl alcohol before being dried in a vacuum oven. The ITO glass was treated with air-plasma (PDC-32G, Harrick plasma) for 10 min at 60 W. The resulting substrates were then baked at 140 °C for 10 min in a N_2 filled glovebox. To compare the performance of a common BHJ system containing a PEDOT:PSS layer, a 30 nm-thick PEDOT:PSS (PH500, H.C. Starck) layer was spin-coated on the air-plasma treated ITO glass and the resulting substrates were also baked at 140 °C for 10 min. The photoactive layer was prepared by dissolving P3HT (Rieke metals with 4002-EE) and PCBM (nano-C (99.5%)) in 1,2-dichlorobenzene (ODCB, Aldrich, anhydrous, boiling point 454 K) and in chlorobenzene (CB, Aldrich, anhydrous, boiling point 404 K) at a 1:0.7 ratio. The solutions were stirred for 12 h at 80 °C to produce a homogeneous blend and were filtered using a 45 μm PTFE filter. For fabrication of the slow dried samples, the photoactive solution, which was dissolved in ODCB, was spin coated at 700 rpm for 40 s on the PEDOT:PSS layer and plasma-treated ITO glass, retaining some residual solvent in the film. Then, the devices were dried in a Petri dish to slowly evaporate the residual solvent over 30 min. This slow-dried sample was annealed at 150 °C for 10 min for further optimization. The devices were then moved from the glovebox to a thermal evaporator for the deposition of cathode materials. At a maximum pressure of 10^{-7} Torr, about 25 nm of calcium and 100 nm of aluminum were deposited sequentially. For fast dried samples, the blend solution, which was dissolved in CB, was spin coated on the PEDOT:PSS layer and the air-plasma treated ITO surface at 1200 rpm for 60 s. The 100 nm aluminum electrode was deposited on the active layer. Thermal annealing was carried out on a digitally controlled hot plate at 150 °C for 10 min to optimize the blend morphology. The active area of each solar cell was 9.9 mm^2.

A hole-only device was fabricated by replacing the metal cathode with a high work function gold electrode to block the injection of electrons from the metal cathode. At a maximum pressure of 10^{-7} Torr, 100 nm of gold electrode was deposited on the active layers at high vacuum condition.

Characterization. A solar simulator (Newport) with a 300 W xenon lamp and an AM1.5G global filter was used. The light intensity was calibrated using a silicon photovoltaic reference cell (Bunkou Keiki Co., BS-520). The current−voltage characteristic curves were measured with a Keithley 236 source measurement unit. The edges of photoactive area are cut by a sharp diamond knife to reduce the charge collection from outside of cells though the high conductive PEDOT:PSS layer. The current was swept from minus to plus direction and the voltage step is 0.02 V. The electrical properties of the ITO surface were obtained using atomic force microscopy (AFM) with a conductive antimony doped Si tip which has a resistivity range of 0.01−0.025 Ω/cm (Bruker, multimode 8). The chemical compositions of various ITOs were analyzed using X-ray photoelectronic spectroscopy (XPS) with a monochromatic Al Kα source at a photon energy of 1486.6 eV (ESCA 2000, Thermo VG scientific). Dynamic secondary ion mass spectroscopy (Magnetic sector SIMS, CAMECA, IMS 7f) was carried out at the National Nano Fab Center in KAIST. The work function of the ITO film was measured using ultraviolet photoelectron spectroscopy (sigma probe, thermo VG scientific) with a 21.2 eV He(I) excitation source.

RESULTS AND DISCUSSION

To investigate the work function and electrical homogeneity of the air-plasma (AP) treated ITO surface, ultraviolet photoelectron spectroscopy (UPS) and conductive tip AFM (c-AFM) measurements were carried out. Prior to the air-plasma treatment, ITO was sequentially cleaned by sonication in acetone, deionized water, and isopropyl alcohol. Then, the solvent-cleaned (SC) ITO surface was subsequently exposed to rf-plasma (air, 60 W) for 10 min using a Harrick model PDC-32G. The UPS result in Figure 1a shows that the work function of SC ITO (4.65 eV) is very different from the highest occupied molecular orbital (HOMO) level of P3HT (~5.0 eV), indicating a nonohmic contact.[21] However, after air-plasma treatment of the ITO surface, the work function increased considerably from 4.65 to 5.12 eV. In other words, the work function energy difference between ITO and the HOMO of P3HT was reduced from 0.35 to 0.12 eV after air-plasma treatment (Figure 1b), suggesting ohmic contact at the anode interface.

Table 1. Work Function of the Solvent-Treated ITO Surface and the Solvent-Cleaned/Air Plasma Treated ITO Surface

	solvent-cleaned ITO	solvent-cleaned/air-plasma-treated ITO (10 min)
Work function (eV)	4.65	5.12

The electrical homogeneity of ITO and air-plasma treated ITO surfaces were further examined using conductive AFM (c-AFM) with a conductive antimony doped Si tip in the resistivity range of 0.01−0.025 Ω/cm. c-AFM images of ITO (Figure 1c) and air-plasma treated ITO surfaces (Figure 1d) show that the areas of higher conductivity, known as "hot spots", and overall electrical homogeneity increased significantly after air-plasma treatment.

This change in the electrical property of ITO can be attributed to the atomic composition change after air-plasma treatment of the ITO surface. This was confirmed using X-ray photoelectron spectroscopy (XPS) (Figure 1e). After air-plasma treatment, the oxygen concentration increased from 55.8% to 63.2%, and the carbon concentration decreased from 19.1% to 10.0% (Table 2). Therefore, it is likely that the

Table 2. Atomic Concentration of the Solvent-Cleaned ITO and the Solvent-Cleaned/Air-Plasma-Treated ITO Surface, As Determined from XPS Spectra

	Atomic concentration (%)			
	C $1_{s1/2}$	O $1_{s1/2}$	Sn $3_{d5/2}$	In $3_{d5/2}$
solvent-cleaned ITO	19.08	55.75	2.91	22.26
solvent-cleaned/air plasma treated ITO	10.01	63.16	3.24	23.59

increased electronegative oxygen and the decreased electron-donating carbon on the air-plasma treated ITO surface repels free electrons in the conduction band, thus leading to a surface depletion region and consequently, a shift in the Fermi level.[25,28] Also, the ratio of the carbon/indium peak intensities reduced significantly from 0.85 to 0.43 after air-plasma treatment (Table 2), indicating that air-plasma treatment is very effective for removing organic residues from the ITO surface.[24,25,29] Therefore, the enhanced uniformity of the

electrical response of the air-plasma treated ITO is attributed to the reduction of carbon contamination. Accordingly, the air-plasma treated ITO surface is capable of creating an ohmic contact to the P3HT donor material with a significantly increased electroactive surface area and without a HTL.

Even though plasma treatment ensures improved hole injection into the ITO anode without a HTL, the hydrophilicity of the plasma treated ITO surface induces interfacial instability and a decohesive force between the anode and hydrophobic photoactive layer, especially at the elevated temperatures. This leads to excessive phase separation of the donor and acceptor material, consequently reducing the performance of the OPVC.[22,26] To reduce excessive phase separation at the anode interface, we controlled the drying condition of the photoactive film on the air-plasma treated ITO. In fact, the thermodynamic stability of the blend film affects the phase separation at elevated temperatures, especially at the interface between the anode and the photoactive layer.[27] To do this, high-boiling point (180.5 °C) dichlorobenzene was used to spin-coat the photoactive materials on the plasma-treated ITO surface. Thus, dichlorobenzene slowly dries and some residual solvent remains in the film after spin-casting. Then, the photoactive layer was dried in a Petri dish to slowly evaporate the residual solvent for 30 min. To compare the effect of the solvent drying on the phase-separation of the active layer, we also used relatively low boiling point (131 °C) chlorobenzene.

In contrast to dichlorobenzene, chlorobenzene fully evaporated during the spin coating process. After additional thermal annealing at 150 °C for 10 min, the phase separation behaviors at the anode interface were investigated using dynamic secondary ion mass spectroscopy (DSIMS).[30,31] We also compared reference samples which were prepared on the PEDOT:PSS layer with the same procedures.

DSIMS results in Figure 2 show that the carbon/sulfur ratio exhibited a distinct marker for the relative PCBM/P3HT

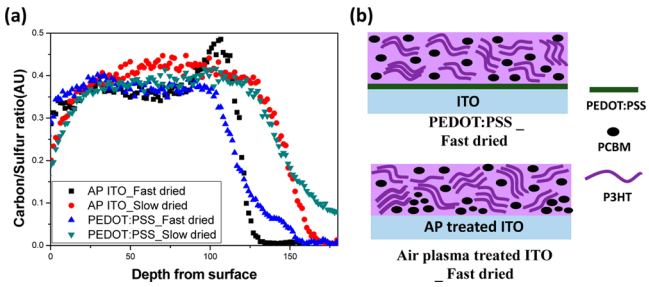

Figure 2. (a) DSIMS data for of the photoactive layer (P3HT/PCBM) on the solvent-cleaned/air plasma-treated ITO and the PEDOT:PSS layer. (b) Schematic illustration of different phase separation of fast dried samples on the PEDOT:PSS layer and air plasma-treated ITO.

composition ratio. We found that the solvent drying conditions significantly affects the phase-separation behavior of the P3HT:PCBM blend. The slow-dried films showed a relatively uniform vertical distribution of P3HT and PCBM on the PEDOT:PSS and air-plasma treated ITO surfaces. However, the fast-dried samples exhibited a very different vertical compositional distribution with regard to anode surfaces: the fast-dried sample on the air-plasma treated ITO surface exhibited a much higher PCBM concentration at the anode interface as compared to those on the PEDOT:PSS layer, indicating extreme phase separation at the anode interface due to the surface energy difference.

It has been reported that the vertical compositional distribution in the P3HT/PCBM blend is attributed to the difference in surface energy between P3HT and PCBM.[27,30] Since PCBM (37.8 Jm^{2-}) has a higher surface energy than P3HT (26.9 Jm^{2-}), PCBM tends to accumulate at a surface with higher surface energy.[30] In contrast, P3HT assembles at a lower surface energy to minimize the overall free energy. Therefore, due to the more hydrophilic nature of air-plasma treated ITO as compared to PEDOT:PSS,[26] more PCBM is likely to be agglomerated at the air-plasma treated ITO interface. However, since the phase of slow-dried film was fully developed during the drying process, the phase separation of the slow-dried films at the elevated temperature was not significantly affected by the surface properties,[27] resulting in a uniform vertical distribution on the air-plasma treated ITO surface. Similarly, a large difference in the vertical phase separation of the fast-dried films suggests that the intermediate morphology of fast-dried films are less stable at elevated temperatures.[27] Therefore, more PCBM molecules in the fast-dried sample were aggregated at the air-plasma ITO interface during thermal annealing because of the higher surface energy of the air-plasma treated ITO surface and the intermediate morphology of the fast-dried film.

To further examine the effect of the solvent drying condition of the photoactive film and the ITO surface on the performance of OPVC, we fabricated devices with fast and slow-dried photoactive layers on ITO and air-plasma treated ITO. As shown in Figure 3, OPVs with clean ITO in the absence of

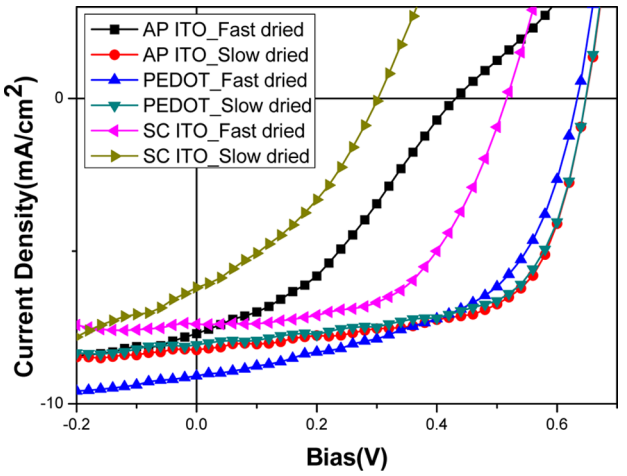

Figure 3. *J*–*V* characteristics of illuminated devices prepared on PEDOT:PSS, solvent-cleaned ITO, and a solvent-cleaned/air plasma treated ITO surface using slow drying (ITO or PEDOT:PSS/active layer/Ca/Al) and fast drying methods (ITO or PEDOT:PSS/active layer/Al).

PEDOT:PSS layer showed poor performance (2.15%, 0.68%), having low values of J_{sc}(7.24 mA/cm^2, 6.20 mA/cm^2), V_{oc}(0.52 V, 0.30 V), and FF(0.57, 0.36). On the other hand, for devices with PEDOT:PSS as an interfacial layer on clean ITO which ensured ohmic contact, enhanced hole collection, electron blocking efficiency, and good performance was exhibited in both slow and fast-dried devices (3.32%, 3.13%). However, devices with air-plasma treated ITO exhibited very different device performance depending on the film preparation method. Slow-dried films prepared on the air-plasma treated ITO showed comparable cell efficiency to that of the PEDOT:PSS

Table 3. Summary of the Averaged Device Operation Parameters from the Light $J-V$ Data in Figure 2

	J_{sc} (mAcm^{-2})	V_{oc} (V)	FF	PCE (%)
SC ITO_SD	7.24 ± 0.32	0.52 ± 0.013	0.57 ± 0.018	2.15 ± 0.14
SC ITO_FD	6.20 ± 0.73	0.30 ± 0.075	0.36 ± 0.097	0.68 ± 0.21
PEDOT:PSS_SD	8.07 ± 0.18	0.65 ± 0.008	0.64 ± 0.016	3.32 ± 0.10
PEDOT:PSS_FD	9.18 ± 0.38	0.63 ± 0.05	0.54 ± 0.024	3.13 ± 0.03
AP ITO_SD	8.24 ± 0.26	0.65 ± 0.02	0.63 ± 0.015	3.38 ± 0.16
AP ITO_FD	7.73 ± 0.22	0.43 ± 0.12	0.36 ± 0.024	1.18 ± 0.41

layer (3.38%) with a short circuit current (J_{sc}) of 8.24 mA/cm^2, an open circuit voltage (V_{oc}) of 0.65 V, and a fill factor of 0.63. Meanwhile, the device with fast-dried active films on the air-plasma treated ITO showed a much lower V_{oc} (0.36 V), J_{sc} (7.73 mA/cm^2), FF (0.36), and power conversion efficiency (1.18%), compared to that with a PEDOT:PSS layer.

The high performance of the slow-dried devices on the air-plasma treated ITO in the absence of a PEDOT:PSS layer is due to the increased work function and electroactive areas, which ensures effective hole extraction at the anode interface, and a uniform vertical compositional distribution. However, the fast-dried active layer on the air-plasma treated ITO showed a much reduced V_{oc}, J_{sc}, and FF, resulting from an S-shaped kink in the photocurrent curve. This is attributed to a carrier extraction barrier induced by interfacial dipole, defects, and traps.[32−34] Therefore, this kink was induced by the nonuniform vertical compositional distribution, indicating that the increased PCBM at the air-plasma treated ITO surface acts as an extraction barrier for hole transport.

To verify the extraction barrier in the fast-dried active layer on the air-plasma treated ITO, the diode property of the device and the hole mobility were measured using a dark $J-V$ curve and a hole-only device, respectively. Figure 4a and Supporting Information Figure S2 show the dark $J-V$ characteristics for cell devices on the PEDOT:PSS, air-plasma treated ITO and solvent-cleaned ITO, over the range of −2 to 2 V. The area normalized currents are plotted on a logarithmic scale. Electrical responses of the slow-dried samples on the PEDOT:PSS and air-plasma treated ITO are similar, showing a low current in the negative quadrant and a high current in the positive quadrant with rectification ratios of ∼5 × 10^2. However, for fast-dried samples, the device on the air-plasma treated ITO showed a much higher reverse bias current and a lower forward bias current with a much reduced rectification ratio of 5, compared to those of the PEDOT:PSS layer on the ITO system. The low rectification ratio of the fast-dried samples on the air-plasma treated ITO was induced by the gradual gradient in the range of 0.5−0.75 V. The linearity of this regime indicates an exponential correlation between the current density and the voltage, which is determined by the diode ideality factor and the reverse saturation current.[35,36] The ideality factor reflects the diode behavior with the applied voltage with regard to its recombination behavior, which takes place where opposing charge carriers meet, that is, the internal interface or the interface between the electrode and the active layer. According to the photoluminescence (PL) results in Supporting Information Figure S1c, d the fast-dried devices on the air-plasma treated ITO showed lower photoluminescence than that on the PEDOT:PSS layer, meaning a lower exciton quenching. Therefore, the poor diode behavior of the fast-dried device on the air-plasma treated ITO may be attributed to the increased recombination at the anode electrode, which arises from the increased PCBM concentration.

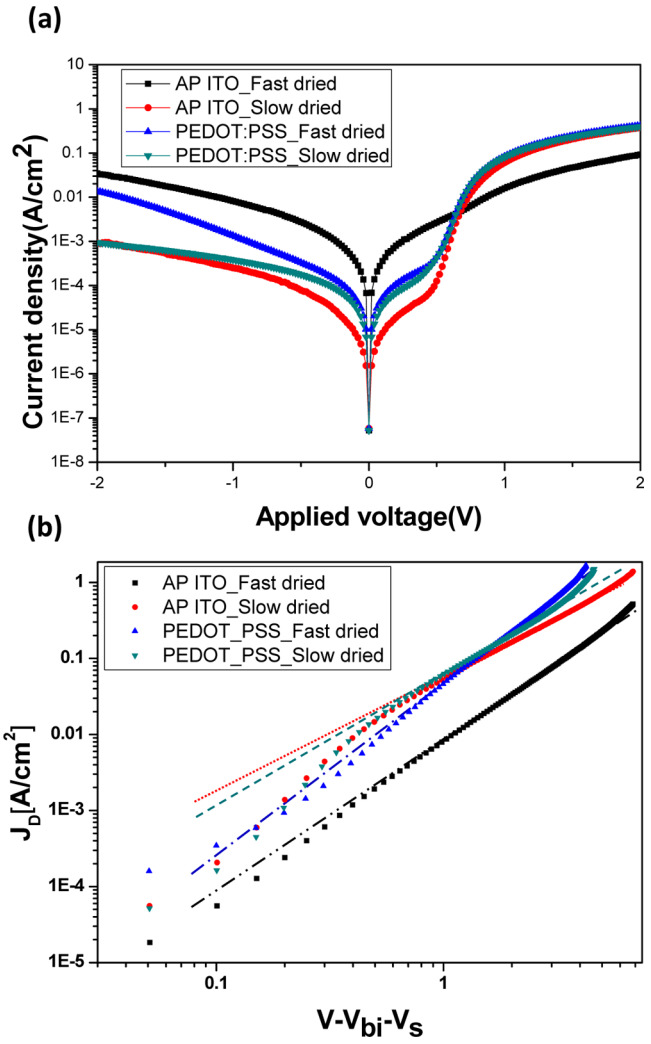

Figure 4. (a) Dark $J-V$ curves of devices prepared using slow dying (SD) and fast drying (FD) methods with solvent-cleaned (SC)/air plasma (AP) treated ITO and a PEDOT:PSS layer. (b) Dark log J–log V curves of hole-only devices prepared by slow drying and fast drying with SC/AP treated ITO and PEDOT:PSS. The bias was corrected for the built-in potential (Vbi) due to the difference between the two electrodes and Vseries. The lines represent the fit to the experimental data using SCLC models.

A hole-only device was fabricated by replacing the metal cathode with a high work function gold electrode to block the injection of electrons from the metal cathode. The mobility of holes was calculated using the space-charge-limited-current (SCLC) model with the equation $J = 9/8\varepsilon_0\varepsilon_r\mu(V^2/L^3)$,[37] where $\varepsilon_0\varepsilon_r$ is the permittivity of the component, μ is the carrier mobility, L is the thickness, and V is the applied voltage. As shown in Figure 4b, for slow-dried devices, the device with air-plasma treated ITO (5.02 × 10^{-4} cm^2/V·S) showed a hole

mobility comparable to the device with PEDOT:PSS (5.25×10^{-4} $cm^2/V{\cdot}S$). However, the fast-dried device on the air-plasma treated ITO (4.48×10^{-5} $cm^2/V{\cdot}S$) showed a much lower hole mobility than that of the PEDOT:PSS layer as a hole transporting layer (3.73×10^{-4} $cm^2/V{\cdot}S$). The hole mobility of OPVC is determined by the crystallinity of the polymer chain and the vertical distribution of the donor and acceptor components.[31,38] As shown in the absorption spectra (Supporting Information Figure S1a and b), the P3HT chains in the fast-dried film (Supporting Information Figure S1b) on the PEDOT:PSS and air plasma treated ITO surface have similar vibronic peak intensities, which correspond to a similar crystallinity in the P3HT chains. Therefore, the low hole mobility of the fast-dried device with air-plasma treated ITO was related to the distribution of P3HT and PCBM within a photoactive layer.

From dark-current and hole mobility results, the low performance (low FF and J_{sc}) of the fast-dried device on the air-plasma treated ITO was attributed to the nonuniform vertical compositional distribution of donor and acceptor materials. The increased PCBM at the air-plasma treated ITO surface acts as an extraction barrier for holes and leads to the S-shaped kink in the J-V curve and low hole mobility. The increased contact area between the PCBM and the ITO anode increases the leakage current and recombination at the anode interface, leading to poor diode properties. In comparison, the slow-dried samples have less interfacial instability due to the thermodynamic stability of slow-dried films at the elevated temperature. Therefore, the slow-dried device on the air-plasma treated ITO has a uniform vertical distribution of P3HT and PCBM even after thermal annealing at a high temperature, thus resulting in high device performance.

CONCLUSIONS

We investigated the effect of air-plasma treatment on the surface of ITO substrates and its implications in the development of high performance PEDOT:PSS free OPVC. After air-plasma treatment, the composition of the ITO surface exhibited increased oxygen and decreased carbon content. Increased electronegative oxygen content resulted in an increased work function of the ITO surface, giving rise to ohmic contact with the P3HT donor material, while a decreased carbon concentration resulted in the enhanced electrical homogeneity of the ITO surface, leading to a reduced charge trap density. From these results, we confirm the possibility of PEDOT:PSS free high performance OPVC using a simple air-plasma treatment. Moreover, the excessive phase separation of the polymer blends on the hydrophilic air-plasma treated ITO was reduced by solvent assisted annealing methods. The slow-dried film showed uniform vertical compositional distribution even after thermal annealing, but the fast-dried film exhibited a large accumulation of PCBM at the anode interface after thermal annealing due to the intermediate morphology. Device performance with air-plasma treated ITO prepared by slow-dried methods showed an efficiency of 3.3%, essentially equaling the performance of a device with a PEDOT:PSS HTL layer. These results show that simple air-plasma treatment of an ITO surface can achieve many of the same effects as a HTL, and that interfacial stability between an ITO surface and a photoactive layer can be reduced by the slow growth methods.

ASSOCIATED CONTENT

Supporting Information

Absorbance spectra of (a) fast dried and (b) slow dried samples on the SC/AP ITO and PEDOT:PSS and photoluminescence spectra of (c) fast dried and (d) slow dried samples on the SC/AP ITO and PEDOT:PSS. This material is available free of charge via the Internet at http://pubs.acs.org.

AUTHOR INFORMATION

Corresponding Author

*Tel: +82-42-350-3931. Fax: +82-42-350-3910. E-mail: heetae@kaist.ac.kr.

Notes

The authors declare no competing financial interest.

ACKNOWLEDGMENTS

This work was supported by the center for advanced Soft Electronics under the Global Frontier Research Program(No, 2011-0032062) funded by the Ministry of Education, Science and Technology, Korea. And this research was supported by the National Research Foundation of Korea(NRF) grant funded by the Korea government(MEST) (No. 2012R1A2A1A01003537)..

REFERENCES

(1) Yu, G.; Gao, J.; Hummelen, J. C.; Wudl, F.; Heeger, A. J. Polymer Photovoltaic Cells: Enhanced Efficiencies via a Network of Internal Donor−Acceptor Heterojunctions. *Science* **1995**, *270*, 1789−1791.

(2) Brabec, C. J.; Sariciftci, N. S.; Hummelen, J. C. Plastic Solar Cells. *Adv. Funct. Mater.* **2001**, *11*, 15−26.

(3) Li, G.; Shrotriya, V.; Huang, J.; Yao, Y.; Moriarty, T.; Emery, K.; Yang, Y. High-Efficiency Solution Processable Polymer Photovoltaic Cells by Self-organization of Polymer Blends. *Nat. Mater.* **2005**, *4*, 864−868.

(4) Kim, J. Y.; Kim, S. H.; Lee, H. H.; Lee, K.; Ma, W.; Gong, X.; Heeger, A. J. New Architecture for High-Efficiency Polymer Photovoltaic Cells using Solution-based Titanium Oxide as an Optical spacer. *Adv. Mater.* **2006**, *18*, 572−576.

(5) Thompson, B. C.; Fréchet, J. M. J. Polymer-Fullerene Composite Solar Cells. *Angew. Chem., Int. Ed.* **2008**, *47*, 58−77.

(6) Jin, J. K.; Choi, J. K.; Hong, Y.; Kang, H.; Yoon, S. C.; Kim, B. J.; Jung, H. T. Synthesis and Photovoltaic Performance of Low-Bandgap Polymers on the Basis of 9,9-Dialkyl-3,6-dialkyloxysilafluorene. *Marcromolecules* **2011**, *44*, 502−511.

(7) Halls, J. J. M.; Walsh, C. A.; Greenham, N. C.; Marseglia, E. A.; Friend, R. H.; Moratti, S. C.; Holmes, A. B. Efficient Photodiodes from Interpenetrating Polymer Networks. *Nature* **1995**, *376*, 498−500.

(8) Cao, Y.; Yu, G.; Zhang, C.; Menon, R.; Heeger, A. J. Polymer Light-Emitting Diodes with Polyethylene Dioxythiophene−Polystyrene Sulfonate as the Transparent Anode. *Synth. Met.* **1997**, *87*, 171−174.

(9) Sun, Y.; Takacs, C. J.; Cowan, S. R.; Seo, J. H.; Gong, X.; Roy, A.; Heeger, A. J. Efficient, Air-Stable Bulk Heterojunction Polymer Solar Cells Using MoO_x as the Anode Interfacial Layer. *Adv. Mater.* **2011**, *23*, 2226−2230.

(10) Irwin, M. D.; Buchholz, D. B.; Hains, A. W.; Chang, R. P. H.; Marks, T. J. p-Type Semiconducting Nickel Oxide as an Efficiency-enhancing Anode Interfacial Layer in Polymer Bulk-heterojucntion Solar Cells. *Proc. Natl. Acad. Sci.* **2008**, *105*, 2783.

(11) Meyer, J.; Hamwi, S.; Bulow, T.; Johannes, H. H.; Riedl, T.; Kowalsky, W. High Efficient Simplified Light Emitting Diodes. *Appl. Phys. Lett.* **2007**, *91*, No. 113506.

(12) So, F.; Kondakov, D. Degradation Mechanisms in Small-molecule and Polymer Organic Light-emitting Diodes. *Adv. Mater.* **2010**, *22*, 3762−3777.

(13) Norrman, K.; Madsen, M. V.; Gevorgyan, S. A.; Krebs, F. C. Degradation Patterns in Water and Oxygen of an Inverted Polymer Solar Cell. *J. Am. Chem. Soc.* **2010**, *132*, 16883−16892.
(14) Jørgensen, M.; Norrman, K.; Krebs, F. C. Stability/Degradation of Polymer Solar Cells. *Sol. Energy Mater. Sol. Cells* **2008**, *92*, 686−714.
(15) Kemerink, M.; Timpanaro, S.; de Kok, M. M.; Meulenkamp, E. A.; Touwslager, F. J. Three-Dimensional Inhomogeneities in PEDOT:PSS Films. *J. Phys. Chem. B* **2004**, *108*, 18820−18825.
(16) Ionescu-Zanetti, C.; Mechler, A.; Carter, S. A.; Lal, R. Semiconductive Polymer Blends: Correlating Structure with Transport Properties at the Nanoscale. *Adv. Mater.* **2004**, *16*, 385−389.
(17) Reynolds, K. J.; Barker, J. A.; Greenham, N. C.; Friend, R. H.; Frey, G. L. Inorganic Solution-Processed Hole-Injecting and Electron-Blocking Layers in Polymer Light-Emitting Diodes. *J. Appl. Phys.* **2002**, *92*, 7556.
(18) Chen, C. P.; Chen, C. P.; Chuang, S. C. High-Performance and Highly Durable Inverted Organic Photovoltaics Embedding Solution-Processable Vanadium Oxides as an Interfacial Hole-Transporting Layer. *Adv. Mater.* **2011**, *23*, 3859−2963.
(19) Zilberberg, K.; Trost, S.; Schmidt, H.; Riedl, T. Solution Processed Vanadium Pentoxide as Charge Extraction Layer for Organic Solar Cells. *Adv. Energy Mater.* **2011**, *1*, 377−381.
(20) Tao, C.; Ruan, S. P.; Xie, G. H.; Kong, X. Z.; Shen, L.; Meng, F. X.; Liu, C. X.; Zhang, X. D.; Dong, W.; Chen, W. Y. Roles of Tungsten Oxide in Inverted Polymer Solar Cells. *Appl. Phys. Lett.* **2009**, *94*, No. 043311.
(21) Irwin, M. D.; Liu, J.; Leever, B. J.; Servaites, J. D.; Hersam, M. C.; Durstock, M. F.; Marks, T. J. Consequences of Anode Interfacial Layer Deletion. HCl-Treated ITO in P3HT:PCBM-Based Bulk-Heterojunction Organic Photovoltaic Devices. *Langmuir* **2010**, *26*, 2584−2591.
(22) Kim, J. S.; Park, J. H.; Lee, J. H.; Jo, J.; Kim, D. Y.; Cho, K. Control of the Electrode Work Function and Active Layer Morphology via Surface Modification of Indium Tin Oxide for High Efficiency Organic Photovoltaics. *Appl. Phys. Lett.* **2007**, *91*, No. 112111.
(23) Mandoc, M. M.; Kooistra, F. B.; Hummelen, J. C.; de Boer, B.; Blom, P. W. M. Effect of Traps on the Performance of Bulk Heterojunction Organic Solar Cells. *Appl. Phys. Lett.* **2007**, *91*, No. 263505.
(24) Brumbach, M.; Veneman, P. A.; Marrikar, F. S.; Schulmeyer, T.; Simmonds, A.; Xia, W.; Lee, P.; Armstrong, N. R. Surface Composition and Electrical and Electrochemical Properties of Freshly Deposited and Acid-Etched Indium Tin Oxide Electrodes. *Langmuir* **2007**, *23*, 11089−11099.
(25) Armstrong, N. R.; Veneman, P. A.; Ratcliff, E.; Plasencia, D.; Brumbach, M. Oxide Contacts in Organic Photovoltaics: Characterization and Control of Near-Surface Composition in Indium-Tin Oxide (ITO) electrodes. *Acc. Chem. Res.* **2009**, *42*, 1748−1757.
(26) Hains, A. W.; Liu, J.; Martinson, A. B. F.; Irwin, M. D.; Marks, T. J. Anode Interfacial Tuning via Electron-blocking/Hole-Transport Layers and Indium Tin Oxide Surface Treatment in Bulk-Heterojunction Organic Photovoltaic Cells. *Adv. Funct. Mater.* **2010**, *20*, 595−606.
(27) Xu, Z.; Chen, L. M.; Yang, G.; Huang, C. H.; Hou, J.; Wu, Y.; Li, G.; Hsu, C. S.; Yang, Y. Vertical Phase Separation in Poly(3-hexylthiophene):Fullerene Derivative Blends and its Advantage for Inverted Structure Solar Cells. *Adv. Funct. Mater.* **2009**, *19*, 1227−1234.
(28) Yu, H. Y.; Feng, X. D.; Grozea, D.; Lu, Z. H. Surface Electronic Structure of Plasma-treated Indium Tin Oxides. *Appl. Phys. Lett.* **2001**, *78*, No. 2595.
(29) Macdonald, G. A.; Veneman, P. A.; Placencia, D.; Armstrong, N. R. Electrical Property Heterogeneity at Transparent Conductive Oxide/Organic Semiconductor Interfaces: Mapping Contact Ohmicity Using Conducting-Tip Atomic Force Microscopy. *ACS Nano* **2012**, *11*, 9623.
(30) Park, H. J.; Kang, M. G.; Ahn, S. H.; Guo, L. J. A Facile Route to Polymer Solar Cells with Optimum Morphology Readily Applicable to a Roll-to-Roll Process without Sacrificing High Device Performances. *Adv. Energy Mater.* **2010**, *22*, E247−E253.
(31) Chen, D.; Nakahara, A.; Wei, D.; Nordlund, D.; Russel, T. P. P3HT/PCBM Bulk Heterojunction Organic Photovoltaics: Correlating Efficiency and Morphology. *Nano Lett.* **2011**, *11*, 561−567.
(32) Krumar, A.; Sista, S.; Yang, Y. Dipole Induced Anomalous S-Shape *I*−*V* Curves in Polymer Solar Cells. *J. Appl. Phys.* **2009**, *105*, No. 094512.
(33) Zhou, Y.; Cheun, H.; Potscavage, W. J.; Hernandez, C. F., Jr.; Kim, S. J.; Kippelen, B. Inverted Organic Solar Cells with ITO Electrodes Modified with an Ultrathin Al2O3 Buffer Layer Deposited by Atomic Layer Deposition. *J. Mater. Chem.* **2010**, *20*, 6189−6194.
(34) Wang, J. C.; Lu, C. Y.; Hsu, J. L.; Lee, M. K.; Hong, Y. R.; Perng, T. P.; Horng, S. F.; Meng, H. F. Efficient Inverted Organic Solar Cells without an Electron Selective Layer. *J. Mater. Chem.* **2011**, *21*, 5723−5728.
(35) Wandauf, C.; Scharber, M. C.; Schilinsky, P.; Hauch, J. A.; Brabec, C. J. Physics of Organic Bulk Heterojunction Devices for Photovoltaic Applications. *J. Appl. Phys.* **2006**, *99*, No. 104503.
(36) Servaites, J. D.; Ratner, M. A.; Marks, T. J. Organic Solar Cells: A New Look at Traditional Models. *Energy Environ. Sci.* **2011**, *4*, 4410−4422.
(37) Lampert, M. A.; Mark, P. *Current Injection in Solids*; Academic Press: New York, 1970.
(38) Aryal, M.; Trivedi, K.; Hu, W. Nano-Confinement Induced Chain Alignment in Ordered P3HT Nanostructures Defined by Nanoimprint. *ACS Nano* **2009**, *3*, 3085.